J. Fluid Mech. (2000), *vol.* 424, *pp.* 279–301. Printed in the United Kingdom

Internal wave evolution in a space–time varying field

By D. A. HORN[1], L. G. REDEKOPP[2], J. IMBERGER[1] AND G. N. IVEY[1]

[1]Centre for Water Research, The University of Western Australia, Nedlands WA 6907, Australia

[2]Department of Aerospace and Mechanical Engineering, University of Southern California, Los Angeles, CA 90089-1191, USA

(Received 13 September 1999 and in revised form 14 June 2000)

An extended Korteweg–de Vries (KdV) equation is derived that describes the evolution and propagation of long interfacial gravity waves in the presence of a strong, space–time varying background. Provision is made in the derivation for a spatially varying lower depth so that some topographic effects can also be included. The extended KdV model is applied to some simple scenarios in basins of constant and varying depths, using approximate expressions for the variable coefficients derived for the case when the background field is composed of a moderate-amplitude ultra-long wave. The model shows that energy can be transferred either to or from the evolving wave packet depending on the relative phases of the evolving waves and the background variation. Comparison of the model with laboratory experiments confirms its applicability and usefulness in examining the evolution of weakly nonlinear waves in natural systems where the background state is rarely uniform or steady.

1. Introduction

Internal solitary waves are common features in lakes, fjords and coastal oceans (Grimshaw 1998). In the coastal ocean and in fjords they are generated by the steepening of the internal tide (e.g. Holloway 1987) and by tidal flows over sills (e.g. Farmer & Smith 1978; Apel *et al.* 1985). In lakes internal solitary waves evolve from the steepening of some initial large-scale internal wave (e.g. Thorpe, Hall & Crofts 1972; Hunkins & Fliegel 1973; Farmer 1978) and from the interaction of large-scale internal waves with topography (e.g. Thorpe *et al.* 1996).

In all these environments internal solitary waves encounter sloping boundaries where they shoal and break, dissipating most of their energy. In this way internal solitary waves play an important role in energy dissipation and in driving mixing of nutrients, oxygen and other biological agents. Laboratory experiments have shown that the resultant dissipation and mixing is dependent on the size and shape of the incident waves and on of the slope of the boundary (Helfrich 1992; Michallet & Ivey 1999). It is therefore of significant practical importance to be able to model the evolution and propagation of internal solitary waves.

Another feature of lakes, fjords and coastal oceans is they are rarely quiescent; rather there is generally some background shear due to a large-scale flow. This background shear is often periodic, due to tidal forcing or, especially in the case of lakes, a large-scale internal wave. Hence, any long wave or solitary wave packet

necessarily evolves and propagates through some large-scale field which is periodic in both space and time.

The simplest model of the evolution and propagation of solitary waves is the Korteweg–de Vries (KdV) equation (for a review see Miles 1981). The KdV equation has been modified to include the effects of weak, steady background shear (Lee & Beardsley 1974; Maslowe & Redekopp 1980), slowly varying topography (Djordjevic & Redekopp 1978) and a slowly varying current (Zhou & Grimshaw 1989), and slowly varying stratification and depth (e.g. Pelinovskiy, Stepanyants & Talipova 1995). In many instances, however, the background is strongly varying in space and time and none of these approaches is completely satisfactory.

This work focuses on the evolution of a packet of interfacial solitary waves in the presence of a prescribed, strong, space–time varying background. It was largely motivated by the laboratory experiments of Horn, Imberger & Ivey (1999), investigating the degeneration of internal standing waves in lakes. In each experiment a standing wave was generated from an initially tilted interface, representing the tilted thermocline in a lake. In most cases the initial standing wave generated by the tilted interface steepened and evolved into a packet of solitary waves, although some energy remained in a residual larger scale. The residual large-scale wave caused the interface on which the solitary wave packet propagated to heave up and down and, in the context of the analysis that follows, it represents the prescribed, strong, space–time varying background through which the solitary wave packet evolved and propagated. The analysis is carried forward for the simple case of a two-layer stratification, as used in the experimental configuration, since the first vertical mode waves are the strongest signal observed in most lakes and since this simplifies the analytical details. The problem is treated as an initial value problem for internal wave motion in a semi-infinite channel where the background state is a large-scale standing wave and a locally steep distortion of the interface is released at a prescribed phase of the standing wave. What is of particular interest is how the packet evolution proceeds as it experiences space–time variations in the magnitude of the leading-order phase speed, the strength of the nonlinear steepening or rarefaction, and the strength of the leading dispersive effect. That is, how the packet evolves where the leading-order, linear evolution proceeds along an accelerating–decelerating characteristic.

After formulating the problem and deriving the evolution equations, we present a number of applications of the model to illustrate the evolution of a packet of solitary waves in the presence of a background large-scale wave in basins with constant and varying depths. Descriptions of the inverse scattering problem for the tilted interface initial condition and of the standing wave in a basin of variable depth are provided in the Appendices.

2. Problem formulation

The analysis for long-wave evolution in a space–time varying background is set in the context of a two-layer stratification. We suppose that a layer of fluid with depth h_1 and density ρ_1 overlays a heavier layer of depth h_2 and density $\rho_2 > \rho_1$. We assume that the fluids are immiscible and that the motion is inviscid. The two-layer model affords a specific context where the varying background state can be both easily visualized and described analytically. The model also provides a good first-order approximation of the lowest vertical eigenmode for realistic environments in stratified lakes (in which the thermocline is usually thin compared with the total depth), as well as the simplest laboratory model in which the theoretical results can be tested.

It was, in fact, laboratory experiments using a two-layer stratification that originally motivated the analysis presented here.

The analysis is presented entirely in dimensional form so that dimensional consistency and familiar groupings of terms are easily recognized. We assume that the typical wavelength for the local waves (i.e. wave motions superimposed on the large-scale inhomogeneous field) is long compared to the total depth h_1+h_2 so that shallow water theory applies in both layers. A non-dimensional amplitude parameter ϵ is then introduced which measures the amplitude of long waves (relative to the upper-layer depth h_1) evolving on the interface which experiences a large-scale, space–time displacement as part of the background field. Denoting the vertical (or wave-guide) coordinate as z, the horizontal (or propagation) coordinate as x, and the (fast) time by t, we introduce the slow space and time scales (X, T) defined by

$$(X, T) = \epsilon^{3/2}(x, t). \tag{2.1}$$

The terms 'long' and 'slow' should be thought of in reference to the smallest layer depth and the time to travel a distance equal to this depth with the limiting, long-wave phase speed. The scale $T = \epsilon^{3/2}t$ is the familiar time scale for weakly nonlinear, weakly dispersive evolution in systems with a finite limiting phase speed (Drazin & Johnson 1989; Johnson 1997). We assume here that the background field also varies on these scales, including the depth of the lower layer so that $h_2 = h_2(X)$. These are the fastest scales allowable for the inhomogeneous background field if nonlinear and dispersive effects are to contribute to the local wave evolution. If the background field varies on slower scales, the local evolution is described by the usual KdV theory modulated by the varying background. The present choice of scales for the background thus considers the case where the local wave evolution is strongly coupled to the varying background field; local wave evolution is equally influenced by nonlinear steepening, wave dispersion, the background shear and the changing depth.

Since the local wave evolution occurs in the presence of a unit-order variation of the background, the usual (cf. Johnson 1997) characteristic variable θ used to measure time (or distance) relative to the leading-order motion along the linear characteristic (assumed here to define wave propagation to the right) is now written as

$$\theta = \frac{s(X, T)}{\epsilon} - \epsilon^{1/2}t, \tag{2.2}$$

where

$$s(X, T) = \int^{X} \frac{\mathrm{d}X'}{c\,(X', T)}. \tag{2.3}$$

In this multiple scales approach, the evolution along the rightward characteristic and occurring in (x, z, t) is transformed to the extended set of independent variables (θ, X, z, T). The situation in mind here, and which we seek to describe in terms of the indicated scaled coordinates, is illustrated in figure 1 where the physical model and an instantaneous linear characteristic are sketched. The characteristic trajectory experiences an order-one variation on the slow scales (X, T) as determined by the underlying motion of the background state. The dependence of c, and therefore s, on both (X, T) is essential to the present objectives and represents the main extension to KdV theory presented here. Previous theories (cf. Grimshaw 1981, 1998) have exclusively considered spatial inhomogeneities, or stated in another way, space–time variations where the temporal inhomogeneity was slower than the spatial inhomogeneity.

As already noted, the analysis is carried forward in terms of dimensional variables

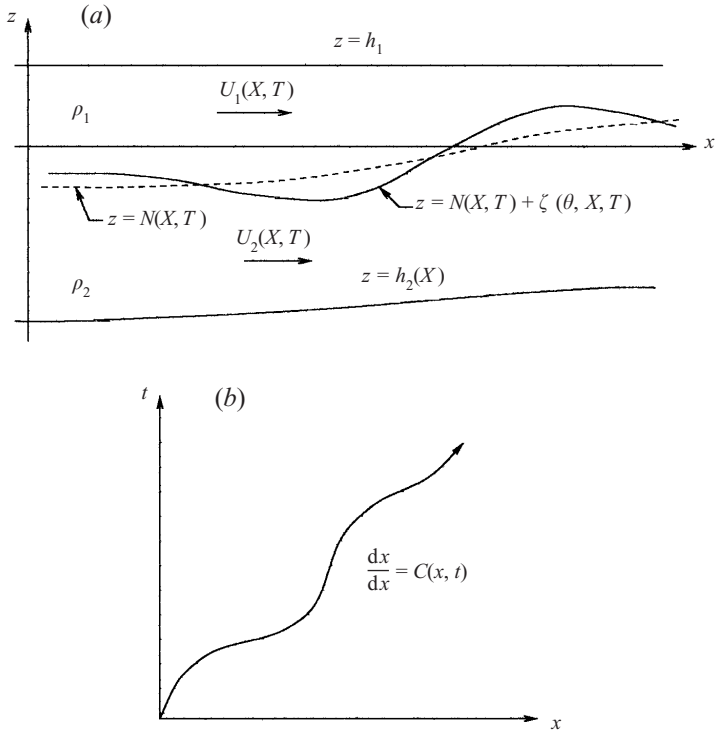

FIGURE 1. Sketch of (*a*) two-layer model with slow space–time-varying ultra-long wave and variable topography, and (*b*) the linear characteristic trajectory in the presence of the varying background.

using the dimensionless amplitude parameter ϵ as the asymptotic order parameter. The dimensional velocities, pressure, and interface displacement, denoted by ($\tilde{}$), are then defined as follows:

$$\left.\begin{aligned} \tilde{u}(x,z,t) &= U(X,z,T) + \epsilon u(\theta,X,z,T;\epsilon),\\ \tilde{w}(x,z,t) &= \epsilon^{3/2} W(X,z,T) + \epsilon^{3/2} w(\theta,X,z,T;\epsilon),\\ \tilde{p}(x,z,t) &= P(X,z,T) + \epsilon p(\theta,X,z,T;\epsilon),\\ \tilde{\zeta}(x,t) &= N(X,T) + \epsilon\zeta(\theta,X,T;\epsilon). \end{aligned}\right\} \tag{2.4}$$

The first set of variables on the right-hand side of each expression represents the space–time varying background which can be thought of as the field induced by an ultra-long wave on the interface (e.g. a large-scale seiche motion upon which local long-wave packets are evolving). The scaling for the vertical velocity $W(X,z,T)$ is consistent with the equation for conservation of mass for the ultra-long wave. The second term in each expression in (2.4) describes the field associated with any local wave evolution and its scaling is consistent with that for weakly nonlinear, weakly dispersive motion of a long wave with amplitude $0 < \epsilon \ll 1$.

In the partitioning of the fields in (2.4) we assume that the ultra-long wave field satisfies the equations of motion in the absence of any local wave evolution. This approximation ignores any loss of energy by the ultra-long wave background as the local field evolves; that is, only a one-way coupling exists by which the background field influences the local evolution and the local evolution does not modify the ultra-long wave. This is admittedly a short-coming of the present theory. However, the

analysis based on this ansatz does provide a means of assessing the effect of a well-defined dynamic straining and advection on the evolution of a solitary wave or an evolving long-wave packet.

The motion of the background plus any local evolving wave packet is described by the equations for a inviscid, incompressible fluid:

$$\left.\begin{aligned} \tilde{u}_x + \tilde{w}_z &= 0, \\ \tilde{u}_t + \tilde{u}\tilde{u}_x + \tilde{w}\tilde{u}_z + \frac{1}{\rho}\tilde{p}_x &= 0, \\ \tilde{w}_t + \tilde{u}\tilde{w}_x + \tilde{w}\tilde{w}_z + \frac{1}{\rho}\tilde{p}_z &= 0. \end{aligned}\right\} \tag{2.5}$$

The pressure $\tilde{p}$ represents the departure of the local pressure from that of the hydrostatically balanced state where the interface is quiescent and at its equilibrium level. The dynamics in either layer must satisfy the kinematic constraint

$$\tilde{w} = \tilde{\zeta}_t + \tilde{u}\tilde{\zeta}_x \quad \text{at} \quad z = \tilde{\zeta} \pm 0, \tag{2.6}$$

relating the dynamic fields to the interface (isopycnal) displacement. We assume $z = 0$ represents the equilibrium level of the interface in the quiescent state. In the inviscid limit, and with immiscible fluids above and below the interface, we also have the normal stress matching condition

$$g(\rho_2 - \rho_1)\tilde{\zeta} + \tilde{p}_1 - \tilde{p}_2 = 0 \quad \text{at} \quad z = \tilde{\zeta}, \tag{2.7}$$

where subscripts 1 and 2 denote, respectively, variables in the upper and lower fluid layers. Employing the ansatz associated with the partitioning of the dependent variables as specified in (2.4), the background field in both layers is described by the following system:

$$\left.\begin{aligned} U_X + W_z &= 0, \\ U_T + UU_X + WU_z - \frac{1}{\rho}P_X &= 0, \\ \frac{1}{\rho}P_z + \epsilon^3\{W_T + UW_X + WW_z\} &= 0, \\ W_{1,2} = N_T + U_{1,2}N_X \quad \text{at} \quad z &= N(X,T), \\ g(\rho_2 - \rho_1)N + P_1 - P_2 = 0 \quad \text{at} \quad z &= N(X,T). \end{aligned}\right\} \tag{2.8}$$

With this formulation the motion of the local wave field defined by the second terms in (2.4) is uniquely specified and is intimately connected to the space–time-varying background.

In what follows we impose the boundary conditions of vanishing normal components of velocity along the level boundary $z = h_1$ for the top layer and $z = h_2(X)$ for the lower layer. The inclusion of topographic effects is straightforward using the present scaling and formulation. To this end, and since we require the ultra-long-wave background field to satisfy the boundary conditions separately, we impose the conditions

$$\left.\begin{aligned} W_1 = w_1 = 0 \quad \text{at} \quad z &= h_1, \\ W_2 = -U_2 h_2'(X), \quad w_2 = -\epsilon u_2 h_2'(X) \quad \text{at} \quad z &= h_2(X). \end{aligned}\right\} \tag{2.9}$$

3. Derivation of the evolution equation

The evolution of local packets of long waves in the presence of a background field (U, W) described by (2.8) is described by means of an asymptotic analysis for $0 < \epsilon \ll 1$. The analysis presented here parallels standard procedures for derivation of the KdV equation, but some important new effects emerge in this inhomogeneous case. Nevertheless, a number of the algebraic details will be omitted and only some of the main intermediate results will be noted.

The dependent variables u, w, ζ and p defined in (2.4) are all expanded in terms of perturbation series. For example, the local interface distortion relative to the background displacement $N(X, T)$ is expressed as

$$\zeta(\theta, X, T; \epsilon) = \zeta^{(1)}(\theta, X, T) + \epsilon\zeta^{(2)}(\theta, X, T) + \cdots. \tag{3.1}$$

In this representation, the velocity components and the pressure appearing in the kinematic condition (2.6) and matching condition (2.7) are expanded in a Taylor series about the equilibrium interface position $z = N(X, T)$. That is, we linearize the interface conditions about the background or ultra-long-wave position.

The equations of motion for the local wave field are obtained by rewriting (2.5) in terms of the scaled coordinates defined in (2.1), (2.2) and (2.3), substituting (2.4) into (2.5), and employing the description of the ultra-long-wave field given in (2.8). Then, expansions of the form (3.1) for the all field variables are employed in the resulting equations. The leading-order set of equations obtained by applying the limit process $\epsilon \to 0$ yield the following solutions for the field variables:

upper layer

$$u_1^{(1)} = V_1(\theta, X, T) = -\frac{C - U_1}{h_1 - N}\zeta^{(1)}, \tag{3.2a}$$

$$w^{(1)} = -\frac{1}{c}V_{1\theta}(z - h_1), \tag{3.2b}$$

$$p_1^{(1)} = \rho_1(C - U_1)V_1. \tag{3.2c}$$

lower layer

$$u_2^{(1)} = V_2(\theta, X, T) = \frac{C - U_2}{h_2 + N}\zeta^{(1)}, \tag{3.3a}$$

$$w_2^{(1)} = -\frac{1}{c}V_{2\theta}(z + h_2), \tag{3.3b}$$

$$p_2^{(1)} = \rho_2(C - U_2)V_2. \tag{3.3c}$$

The variable C appearing in these solutions is defined as

$$C(X, T) = c(1 - s_T) = c(X, T)\left\{1 - \frac{\partial}{\partial T}\int^X \frac{\mathrm{d}X'}{c(X', T)}\right\}, \tag{3.4}$$

where $c(X, T)$, the long-wave phase speed, is the eigenvalue of the leading-order linear system which varies slowly in space and time in accordance with the background state. One may note that the expression for $C(X, T)$ is related to the characteristic phase function $\theta(x, t)$ in (2.2), $C = -\theta_t/\theta_x$, but we prefer to present the analysis which follows in terms of the two related functions $c(X, T)$ and $C(X, T)$.

The eigenvalue relation is obtained by using (3.2) and (3.3) in the leading-order pressure matching condition (2.7). Substituting into the resulting matching condition

yields the result

$$\rho_1 \frac{(C-U_1)^2}{h_1-N} + \rho_2 \frac{(C-U_2)^2}{h_2+N} - g(\rho_2-\rho_1) = 0. \tag{3.5}$$

The analytic form of this expression is very familiar as the long-wave limit of the dispersion relation for the Kelvin–Helmholtz instability problem (in the absence of surface tension effects) insofar as the variable $C(X,T)$ is concerned (Drazin & Reid 1981). There is, however, a fundamental difference in that (3.5) is not a quadratic polynomial for the eigenvalue, but an integro-differential equation for the phase speed $c(X,T)$, as is seen from (3.4). It is the solution of this equation for a prescribed background state that determines the trajectory of the linear characteristic for local wave evolution which was sketched in figure 1. When U_1, U_2, N and h_2 are constant, $s_T = 0$ and we recover the familiar quadratic relation for the phase speed c.

Carrying the asymptotic expansion forward to second order, a compatability condition emerges describing the evolution of the leading-order displacement function $\zeta^{(1)}(\theta, X, T)$. As the analytical procedures are well established, the algebraic steps are suppressed and the detailed form of the modified KdV equation describing the evolution of the local interface displacement $\zeta^{(1)}$ in the presence of the inhomogeneous, non-stationary background is given in Appendix A as it emerges in the $O(\epsilon)$ closure. The equation is expressed here in the abbreviated form

$$\zeta^{(1)}_T + C\zeta^{(1)}_X + n(X,T)\zeta^{(1)} + \frac{1}{c}\alpha(X,T)\zeta^{(1)}\zeta^{(1)}_\theta + \frac{1}{c^3}\beta(X,T)\zeta^{(1)}_{\theta\theta\theta} = 0. \tag{3.6}$$

The more lengthy expression appearing in equation (A 1) for the index-of-refraction term $n(X,T)$ can be written compactly as

$$n(X,T) = C_X + \frac{1}{2D}(D_T + CD_X), \tag{3.7}$$

where the quantity $D(X,T)$ has the definition

$$D(X,T) = \rho_1 \frac{C-U_1}{h_1-N} + \rho_2 \frac{C-U_2}{h_2+N}. \tag{3.8}$$

We note that for the special limit of variable depth $h_2(X)$, but with $U_1 = U_2 = N = 0$, the index of refraction assumes the form

$$n(X) = \tfrac{1}{2}C_X = \tfrac{1}{2}c_X = \frac{c}{4}\frac{\rho_2 h_1}{\rho_1 h_2 + \rho_2 h_1}\frac{h_2'}{h_2}. \tag{3.9}$$

This limiting form for long-wave propagation in a spatially inhomogeneous medium, where the inhomogeneity derives from a spatially varying wave-guide dimension, is consistent with results obtained by Kakutani (1971) and Johnson (1973) for free-surface gravity waves and by Djordjevic & Redekopp (1978) for internal waves in a two-layer system. For the limiting case just described, where the index of refraction is independent of time, the dependence of $\zeta^{(1)}$ on the slow time scale $T = \epsilon^{3/2}t$ vanishes and $\zeta^{(1)} = \zeta^{(1)}(\theta, X)$ and $C(X) = c(X)$. Equation (3.6) then reduces to the form given in Djordjevic & Redekopp (1978).

It is convenient for laboratory comparisons to have the evolution equation recast in terms of laboratory coordinates and the unscaled interface displacement. In terms of these original variables (3.6) becomes

$$\zeta_t + C(x,t)\zeta_x + n(x,t)\zeta + \alpha(x,t)\zeta\zeta_x + \beta(x,t)\zeta_{xxx} = 0. \tag{3.10}$$

It is worth noting that the solution of (3.10) does not require explicit computation of

the phase speed $c(x,t)$. The speed function $C(x,t)$, which can be computed directly from (3.5), is now related to $c(x,t)$ by

$$C(x,t) = c(x,t)\,(1-s_t) = c(x,t)\left\{1 - \frac{\partial}{\partial t}\int^{x} \frac{\mathrm{d}x'}{c\,(x',t)}\right\}. \tag{3.11}$$

The index of refraction, however, when written explicitly in terms of the field variables can be related to spatial or temporal gradients of the base state separately as follows:

$$n(x,t) = n^{(t)} + n^{(x)}, \tag{3.12a}$$

where

$$n^{(t)} = \frac{\rho_1\rho_2\,(U_1-U_2)\,(U_{2t}-U_{1t})}{2D^2\,(h_1-N)\,(h_2+N)} + \left\{\rho_1\frac{C-U_1}{(h_1-N)^2} - \rho_2\frac{C-U_2}{(h_2+N)^2} + \frac{\rho_1\rho_2\,(U_1-U_2)}{D\,(h_1-N)\,(h_2+N)}\left[\frac{C-U_1}{h_1-N} + \frac{C-U_2}{h_2+N}\right]\right\}\frac{N_t}{4D} \tag{3.12b}$$

and

$$\begin{aligned} n^{(x)} = {} & \frac{\rho_1\rho_2\,(U_1-U_2)\,(U_{2x}-U_{1x})}{2D^2\,(h_1-N)\,(h_2+N)} + \frac{1}{D}\left\{\rho_1\frac{C-U_1}{h_1-N}U_{1x} + \rho_2\frac{C-U_2}{h_2+N}U_{2x}\right\} \\ & + \left\{\rho_2\frac{(C-U_2)\,(C-2U_2)}{(h_2+N)^2} - \rho_1\frac{(C-U_1)\,(C-2U_1)}{(h_1-N)^2} \right. \\ & \left. + \frac{\rho_1\rho_2 C\,(U_1-U_2)}{D\,(h_1-N)\,(h_2+N)}\left[\frac{C-U_1}{h_1-N} + \frac{C-U_2}{h_2+N}\right]\right\}\frac{N_x}{4D} \\ & + \frac{\rho_2}{4D}\frac{C-U_2}{(h_2+N)^2}\left\{(C-2U_2) - \frac{\rho_1 C\,(U_1-U_2)}{D\,(h_1-N)}\right\}h_2'(x). \end{aligned} \tag{3.12c}$$

Each term is proportional to the respective gradient of the inhomogeneous background or ultra-long-wave field.

To further illuminate the implications of the variable-coefficient KdV equation (3.10), we form an equation for an integral measure of the local 'energy' appropriate for an initial value problem on the unbounded line. Multiplying (3.10) by ζ and integrating over the infinite spatial domain yields

$$\frac{1}{2}\frac{\partial}{\partial t}\int_{-\infty}^{\infty}\zeta^2\mathrm{d}x = -\int_{-\infty}^{\infty}\left\{\left(n-\tfrac{1}{2}C_x\right)\zeta^2 - \tfrac{1}{3}\alpha_x\zeta^3 + \tfrac{1}{2}\beta_x\left[\tfrac{3}{2}\zeta_x^2 - \left(\zeta^2\right)_{xx}\right]\right\}\mathrm{d}x. \tag{3.13}$$

The familiar conservation law for the standard KdV equation is recovered in the limit of a homogeneous background state when $n = C_x = \alpha_x = \beta_x = 0$. Since the sign of the integrand on the right-hand side changes locally in space and time, this particluar measure of the energy in a wave packet shows that the wave amplitude will either increase or decrease locally as it propagates through a space–time-varying background field. Also, since derivatives of the different coefficient functions appear in the integrand on the right-hand side, energy transfer to or from the long wave will depend crucially on the phase of the ultra-long-wave field. We point out that the first term in the integral on the right-hand side vanishes for the special case represented by (3.9). In the general case of an arbitrary inhomogeneous background field this coefficient can be written in the compact form

$$n - \frac{C_x}{2} = \frac{1}{2D}\left\{D_t + (CD)_x\right\}, \tag{3.14}$$

where D is defined in (3.8).

The terms involving the nonlinear and dispersive coefficients α and β appearing in the integral on the right-hand side of (3.13) are of higher order than the index-of-refraction term when the integral is recast using the asymptotic expansion. When these terms are neglected, for example in (3.6), an alternative energy density can be defined leading to the relation

$$\frac{\partial}{\partial T}\int_{-\infty}^{\infty} CD\zeta^{(1)^2}\mathrm{d}X = \int_{-\infty}^{\infty} C_T D\zeta^{(1)^2}\mathrm{d}X. \tag{3.15}$$

This expression is an extension of that given, for example, by Grimshaw (1998), and reveals the special consequence of a non-stationary background state. If the background is inhomogeneous, but stationary, one obtains the familiar conservation of wave action flux.

4. Evolution in the presence of moderate inhomogeneity

The derivation of the evolution equation in the previous section was premised on the existence of a unit-order, large-scale background wave field. The resulting evolution equation (3.10), together with the eigenvalue relation defined by (3.5) and (3.11), can be subsequently used as a basis for analysing the evolution of a long-wave packet in the limit of a moderate-amplitude background state. To make the relative strength of this state explicit, we introduce the dimensionless scale parameter δ where we suppose that $|N(x,t)| = O\left(\delta h_{1,2}\right)$ and where $0 < \epsilon \ll \delta < 1$. At the same time we suppose that the large-scale velocity field $U_{1,2}$ derives solely from the large-scale interface displacement $N(x,t)$. That is, we exclude the case where an imposed, order-one, parallel shear flow exists in addition to the flow induced by the displacement $N(x,t)$. Hence, $U_{1,2}$ will also be of order δ relative the phase speed of infinitesimal waves propagating on the interface.

Formal development of the modified evolution problem for the limit case defined above proceeds by defining the parameter expansions

$$\left.\begin{aligned} c &= c_0 + \delta c_1 + \cdots, \\ C &= C^{(0)} + \delta C^{(1)} + \cdots, \\ N &= \delta N^{(1)} + \delta^2 N^{(2)} + \cdots, \\ U_{1,2} &= \delta U_{1,2}^{(1)} + \delta^2 U_{1,2}^{(2)} \ldots \ . \end{aligned}\right\} \tag{4.1}$$

Substitution of these expansions into (3.5) and (3.11) yields the relations

$$C^{(0)^2} = c_0^2 = \frac{g\,(\rho_2 - \rho_1)\,h_1 h_2}{\rho_1 h_2 + \rho_2 h_1}, \tag{4.2}$$

$$C^{(1)} = \frac{c_0}{2h_1 h_2}\frac{\rho_2 h_1^2 - \rho_1 h_2^2}{\rho_1 h_2 + \rho_2 h_1}N^{(1)} + \frac{\rho_1 h_2 U_1^{(1)} + \rho_2 h_1 U_2^{(1)}}{\rho_1 h_2 + \rho_2 h_1}. \tag{4.3}$$

The first correction to the phase speed c_1 requires solution of the integro-differential equation

$$c_1 + c_0\frac{\partial}{\partial t}\int^{X}\frac{c_1\,(x',t)\,\mathrm{d}x'}{c_0^2\,(x')} = C^{(1)}(x,t). \tag{4.4}$$

However, and as pointed out earlier, the explicit solution for c_1 is not required to obtain the approximate form of the coefficients of (3.10) correct to $O(\delta)$ nor for the

solution of the resulting limit of the evolution equation. Calculation of the coefficient functions in (3.10) correct to $O(\delta)$, although a bit tedious, leads to the following expressions:

$$n = \frac{c_0}{4}\frac{\rho_2 h_1}{\rho_1 h_2 + \rho_2 h_1}\frac{h_2'(x)}{h_2} + \delta\left\{\frac{1}{4}\frac{\rho_1 h_2^2 - \rho_2 h_1^2}{\rho_1 h_2 + \rho_2 h_1}\cdot\frac{N_t^{(1)}}{h_1 h_2} + \frac{\rho_1 h_2 U_{1x}^{(1)} + \rho_2 h_1 U_{2x}^{(1)}}{\rho_1 h_2 + \rho_2 h_1}\right.$$
$$+\left[\frac{1}{2}\frac{\rho_1 h_2^2 - \rho_2 h_1^2}{\rho_1 h_2 + \rho_2 h_1}\frac{N^{(1)}}{h_1 h_2} - 2\frac{\rho_1 h_2}{\rho_1 h_2 + \rho_2 h_1}\cdot\frac{h_2 - h_1}{h_1 h_2}N^{(1)} - \frac{\rho_1 h_2 U_1^{(1)} + \rho_2 h_1 U_2^{(1)}}{c_0(\rho_1 h_2 + \rho_2 h_1)}\right.$$
$$\left.\left.+2\frac{\rho_1 h_2\left(U_1^{(1)} - U_2^{(1)}\right)}{c_0(\rho_1 h_2 + \rho_2 h_1)}\right]\frac{c_0}{4}\frac{\rho_2 h_1}{\rho_1 h_2 + \rho_2 h_1}\frac{h_2'(x)}{h_2}\right\} + O\left(\delta^2\right), \tag{4.5}$$

$$\alpha = \frac{3c_0}{2h_1 h_2}\cdot\frac{\rho_2 h_1^2 - \rho_1 h_2^2}{\rho_1 h_2 + \rho_2 h_1} + \frac{3\delta}{h_1 h_2}\left\{\frac{c_0}{h_1 h_2}\left[\frac{3}{4}\left(\frac{\rho_2 h_1^2 - \rho_1 h_2^2}{\rho_1 h_2 + \rho_2 h_1}\right)^2 - \frac{\rho_2 h_1^3 + \rho_1 h_2^3}{\rho_1 h_2 + \rho_2 h_1}\right]N^{(1)}\right.$$
$$\left.+\frac{\rho_1 h_2^2 U_1^{(1)} - \rho_2 h_1^2 U_2^{(1)}}{\rho_1 h_2 + \rho_2 h_1} + \frac{\rho_2 h_1^2 - \rho_1 h_2^2}{\rho_1 h_2 + \rho_2 h_1}\cdot\frac{\rho_1 h_2 U_1^{(1)} + \rho_2 h_1 U_2^{(1)}}{\rho_1 h_2 + \rho_2 h_1}\right\} + O\left(\delta^2\right), \tag{4.6}$$

$$\beta = \frac{c_0}{6}h_1 h_2\frac{\rho_1 h_1 + \rho_2 h_2}{\rho_1 h_2 + \rho_2 h_1} + \delta\left\{\frac{c_0}{6}\left[\frac{(\rho_2 - \rho_1)h_1 h_2}{\rho_1 h_2 + \rho_2 h_1} + \frac{3}{2}\frac{\rho_1 h_1 + \rho_2 h_2}{\rho_1 h_2 + \rho_2 h_1}\cdot\frac{\rho_2 h_1^2 - \rho_1 h_2^2}{\rho_1 h_2 + \rho_2 h_1}\right]N^{(1)}\right.$$
$$\left.+\frac{1}{3}h_1 h_2\left[\frac{\rho_1 h_1 + \rho_2 h_2}{\rho_1 h_2 + \rho_2 h_1}\cdot\frac{\rho_1 h_2 U_1^{(1)} + \rho_2 h_1 U_2^{(1)}}{\rho_1 h_2 + \rho_2 h_1} - \frac{\rho_1 h_1 U_1^{(1)} + \rho_2 h_2 U_2^{(1)}}{\rho_1 h_2 + \rho_2 h_1}\right]\right\} + O\left(\delta^2\right). \tag{4.7}$$

The foregoing expressions can be used in (3.10) to describe approximately the evolution of a long internal wave in the presence of a moderate-amplitude ultra-long wave. Retaining terms up to the level of approximation used in the expansions for the coefficient functions given above, the wave motion is asymptotically correct to $O(\delta^2\epsilon, \epsilon^2)$ where ϵ is the amplitude of the evolving long-wave packet and δ is the amplitude of the background ultra-long-wave field. Insofar as (3.10) is an unscaled, dimensional equation for the interface distortion $\zeta(x,t)$, and that δ was introduced only to provide a systematic basis for the calculation of approximate forms for the coefficients C, n, α, and β, the parameter δ can be simply combined with the first-order functions $N^{(1)}$ and $U_{1,2}^{(1)}$ to represent the available dimensional fields $N(x,t)$ and $U_{1,2}(x,t)$. These fields can then be used directly in computing C from (4.1), (4.2) and (4.3) and n, α, and β from (4.5), (4.6) and (4.7). In this way the weakly nonlinear, weakly dispersive evolution of a local long-wave packet in the presence of a space–time varying background field of moderate amplitude is completely specified within the order of approximation defined above.

5. Applications

5.1. *Evolution in a basin of uniform depth*

In this section we consider two specific applications of the model equation derived here describing the evolution of long waves in the presence of a moderate-amplitude ultra-long wave. To do this we solve (3.10) using a pseudospectral method similar to

that described by Fornberg & Whitham (1978). The variable coefficients described by (4.3), (4.5), (4.6) and (4.7) are calculated over the whole domain for each time step.

Case 1: Evolution of a depression of the interface

We first examine the evolution of a disturbance of the interface at the origin as it propagates into a periodically varying background on a semi-infinite domain. Such a situation arises when wind blows over a lake for a time shorter than $T_0/4$, where $T_0 = 2L/c_0$ is the period of the first horizontal mode internal wave (Spigel & Imberger 1980), also referred to as the internal seiche. The applied wind stress results in a depression of the thermocline at the downwind end of the lake and a corresponding elevation at the upwind end. When the wind stress is removed, the depression propagates as a long wave towards the centre of the lake. If the rate of nonlinear steepening is sufficiently rapid, that is if the wave steepens more quickly than it can be damped, the long wave evolves into a packet of solitary waves. This process generally occurs in the presence of some existing background large-scale wave motion. This scenario is often found in very long lakes where the period of the seiche, T_0, is likely to be much greater than the duration of most wind events (e.g. Farmer 1978).

To demonstrate the influence of the background seiche on the evolution of a depression of the thermocline we allow a triangular disturbance to propagate into a periodically varying background described by a linear wave of amplitude N_0 and wavelength $2L$:

$$\left.\begin{aligned} N(x,t) &= N_0 \cos\left(\frac{\pi x}{L}\right)\cos\left(\frac{\pi}{L}c_0 t\right), \\ U_1(x,t) &= -\frac{N_0 c_0}{h_1}\sin\left(\frac{\pi x}{L}\right)\sin\left(\frac{\pi}{L}c_0 t\right), \\ U_2(x,t) &= \frac{N_0 c_0}{h_2}\sin\left(\frac{\pi x}{L}\right)\sin\left(\frac{\pi}{L}c_0 t\right). \end{aligned}\right\} \tag{5.1}$$

Since we later make direct comparisons of the evolution predicted by the modified KdV equation (3.10) derived here with laboratory experiments, it is important to include in the model dissipative effects arising from laminar boundary layers along the surface of the tank. To this end we employ the extended KdV equation (Keulegan 1948; Miles 1976) applicable to a tank with rigid upper and lower surfaces

$$\begin{aligned} &\zeta_t + C(x,t)\zeta_x + n(x,t)\zeta + \alpha(x,t)\zeta\zeta_x + \beta(x,t)\zeta_{xxx} \\ &\quad = \frac{C^{1/2}}{4\pi}\sqrt{\frac{\nu}{2}}\frac{h_1 + h_2 + 4h_1h_2/b}{h_1h_2}\int_{-\infty}^{\infty}|k|^{1/2}(-1 + \mathrm{i}\,\mathrm{sgn}\,k)\hat{\zeta}(k,t)\,\mathrm{e}^{\mathrm{i}kx}\mathrm{d}k, \end{aligned} \tag{5.2}$$

where b is the width of the tank, ν is the kinematic viscosity of the fluid and $\hat{\zeta}(k,t)$ is the Fourier transform with respect to the propagation distance x.

Figure 2 shows the effect of changing the amplitude and phase of the background wave (note that the plot shows a wave of elevation propagating on a thin lower layer). The peak of the triangular initial condition in figures 2(*a*) and 2(*b*) coincides with the *crest* of the background wave at $t = 0$, so that the disturbance initially evolves on the front face of the background wave. The amplitude of the background wave is 20% of the amplitude of the initial condition in figure 2(*a*) and 10% of the amplitude of the initial condition in 2(*b*). Figure 2(*c*) illustrates the homogeneous case in which there is no background wave and in figures 2(*d*) and 2(*e*) the phase of the seiche is reversed so that the peak of the initial condition coincides with the *trough* of the background wave at $t = 0$.

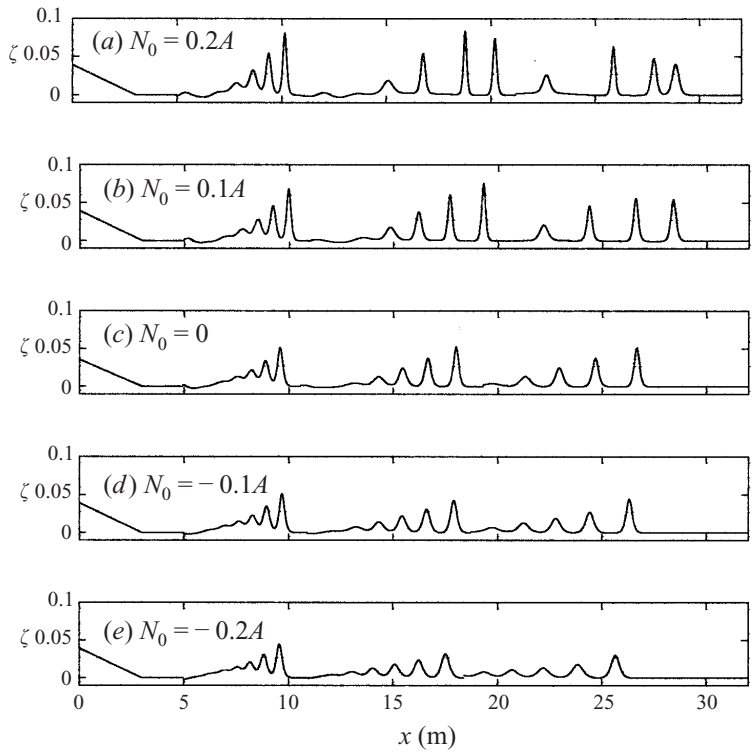

FIGURE 2. Effect of changing the amplitude and the phase of the background seiche on the evolution of a long-wave packet. Seiche wave amplitudes at $x = 0$ are noted on the respective panels. Each panel contains the spatial structure of the packet at the times $t = 0, 50, 100, 150$ s. All simulations have $h_2/H = 0.2$, $\Delta\rho/\rho_2 = 0.02$ and $L = 6$ m.

In the cases where the initial condition coincides with the crest of the background wave (figures 2*a* and 2*b*) the integrand of (3.13) is initially positive and the amplitudes of the evolving solitary waves increase. The rate of change of energy can be calculated from (3.13) and is plotted in figure 3. In these two cases, however, the solitary waves propagate at a greater speed than c_0, gaining on the background wave, so that they eventually move into the trough of the long wave. When this occurs the sign of the integrand in (3.13) changes and the energy of the waves decreases. This happens first to the leading soliton, which is reduced in amplitude and speed, and then to the following waves as they also move into the trough. In figures 2(*d*) and 2(*e*) the disturbance begins in the trough of the long wave and so the integrand of (3.13) is negative. Although the disturbance steepens, it does so more slowly than in the absence of a varying background and the amplitudes of the evolving solitary waves are reduced. However, these evolving solitons still propagate at speeds greater than c_0 and move through the background wave so that the energy integral would eventually become positive whereupon they would increase in amplitude. One observes that the peak wave amplitude, the amplitude distribution in the packet, and the position of the front of the packet are all influenced quite significantly by the presence and strength of the seiche.

In summary, as a packet of solitary waves moves through a strong space–time-varying background field it will either gain or lose energy depending on the phase of the background field. These energy fluxes result in increases and decreases in wave

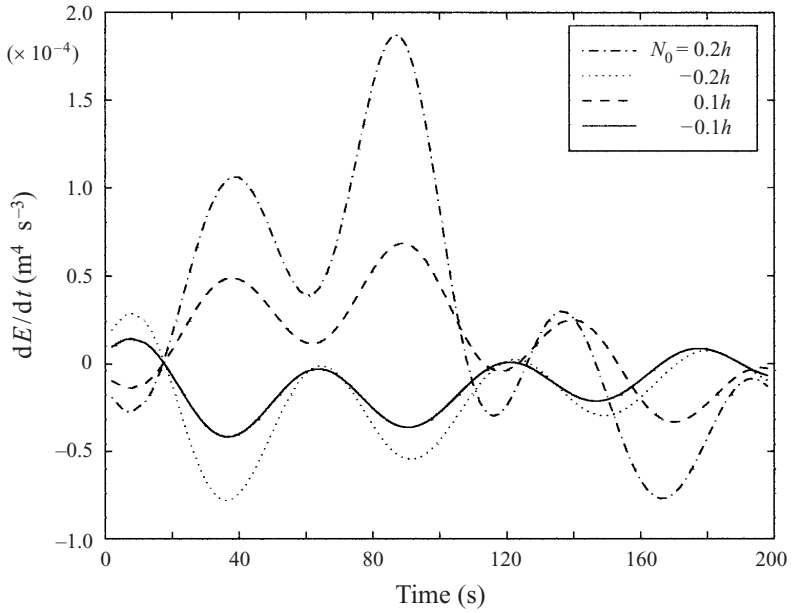

FIGURE 3. Rates of change of the energy as calculated using equation (3.13) for the simulations shown in figure 2.

amplitude and speed that significantly change the character and appearance of the individual waves and of the wave packet.

In order to provide an estimate of the expected number of solitary waves emerging from an initial non-equilibrium state of the form investigated here, the direct scattering portion of the inverse scattering transform (IST) for the KdV equation (cf. Ablowitz & Segur 1981) was solved for a triangular-shaped initial condition. The results are presented in Appendix B.† The IST solution for the chosen initial condition for the results presented in figure 2 predicts the appearance of five solitons. This is consistent with the evolution shown in figure 2(*c*) when no seiche field is present.

Case 2: Application to the evolution of a tilted interface in a closed basin

We next consider the situation when wind blows over the surface of a narrow lake for sufficient time to tilt the thermocline over the length of the lake. This occurs when the duration of the wind event exceeds $T_0/4$ (Spigel & Imberger 1980). This initial condition and its idealization for the purposes of the model, are shown schematically in figure 4. This is the initial condition for the classical internal seiche (eg. Mortimer 1952) and was the initial condition considered by Horn *et al.* (2001) in their study of the degeneration of basin-scale internal waves in lakes.

The relaxation of the initial thermocline tilt in a closed basin necessarily involves wave propagation along both the rightward and leftward families of characteristics. Hence, the description of this relaxation process via a single KdV equation which models waves propagating along only a single characteristic (assumed to the right) requires some explanation. First, we hypothesize that the initial condition can be split into two parts: one giving rise to a propagating packet of long waves and

† Appendix B is available from the Journal of Fluid Mechanics editorial office, Cambridge, and is posted on the web site http://www.cwr.uwa.edu.au/~horn/papers/space-time.html.

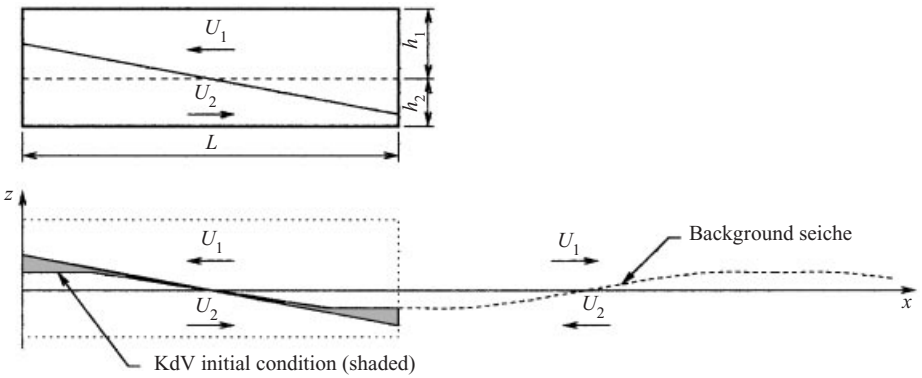

FIGURE 4. Schematic diagram of the KdV model for the extended laboratory domain. The displacement of the tilted interface is partitioned between a background seiche and an initial condition for evolution of a long-wave packet.

the other to a standing wave field. Now, the portioning of the initial state between these components is quite arbitrary. However, the IST analysis presented in Appendix B shows that the number of solitons emerging from an initial condition having adjoining segments of positive and negative volumetric displacement is only slightly affected by the presence of the negative part. This suggests that one might view the positive part as contributing to the evolving wave packet and the negative part to the seiche. Of course, the net volumetric displacement in a closed basin is identically zero and, for this reason, we choose to split the initial condition evenly between the two fields. Second, we neglect the interactions between the two families of characteristics occurring on a fast time scale. Instead we reflect the closed basin of length L about an end (the right-hand end for a right-hand KdV equation), forming a basin of length $2L$, and consider a semi-infinite periodic extension of the reflected basin of length $2L$. We conjecture that this repetitive extension of the basin domain onto the semi-infinite line ($x > 0$) with $2L$ periodicity should provide a reasonable first approximation of the evolving wave field in the closed basin of interest. The advantage of the model proposed here is that it affords a rapid calculation tool for exploring parametric effects in closed basins. We comment that one can add a spatially varying (periodic with period $2L$) dissipative term in the model to simulate effects of shoaling and reflection at an endwall, but we do not pursue such extensions here.

To test the applicability of the extended KdV model, we compare its results with data from one of a series of laboratory experiments carried out by Horn *et al.* (2001). The experimental techniques and results are described in more detail in that work but will be briefly summarized below.

The laboratory experiments were conducted in a clear acrylic tank 6 m long, 29 cm deep and 30 cm wide with an axis of rotation approximately through the tank centre to allow the interface to be initially tilted. The tank was filled with a two-layer stratification ($h_2/H = 0.2$), the upper layer being fresh and the lower layer saline ($\rho \approx 1020\,\mathrm{kg\,m^{-3}}$). The tank was then rotated through a small angle (0.5° for this experiment) to its initial position. The experiment begins at $t = 0$ when the tank is suddenly returned to a horizontal position and baroclinic pressure gradients drive a flow from right to left below the pycnocline and from left to right above it. The ensuing flow was recorded on video and still photographs and by ultra-sonic wavegauges. The experimental set-up and the positions of the two wavegauges are shown in figure 5.

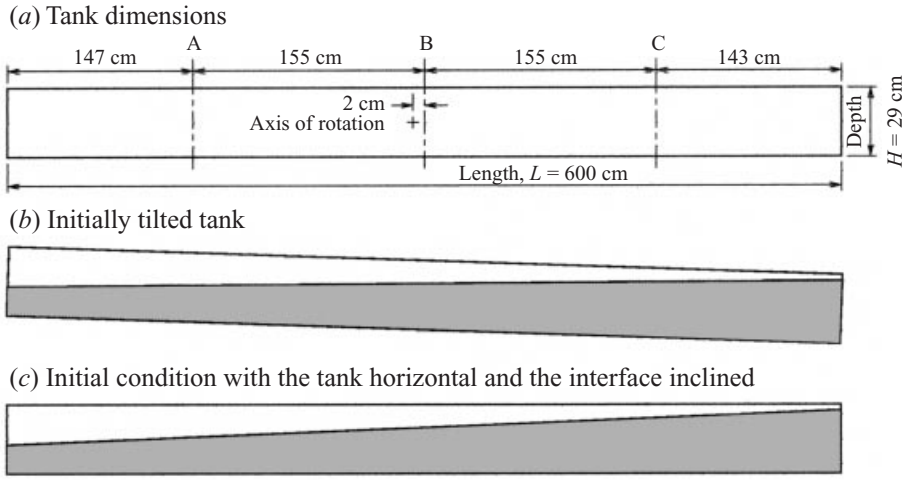

FIGURE 5. Schematic of the laboratory model. Ultrasonic wavegauges are located at the positions marked A, B, and C. The shaded regions in (*b*) and (*c*) show the density structure immediately before and after an experiment commences.

In this experiment (and in most of the experiments conducted by Horn *et al.* 2001), the initial standing wave generated by the tilted interface steepened and evolved into a packet of solitary waves. Not all of the energy of the initial condition was transferred to the solitary waves. Some energy remained in a residual larger-scale wave that heaved the interface, on which the solitary wave packet propagated, up and down. For the purposes of the model, we take the residual large-scale internal wave to be the prescribed, strong, space–time varying background through which the solitary wave packet evolves and propagates. Note that the present model does not provide any rational basis for partitioning the energy resident in an initial, large-scale, non-equilibrium state between an evolving packet of long waves with length scale small compared to L and a residual standing wave. We therefore postulate *ab initio* that a given fraction of this energy will flow directly into a standing wave which extends throughout the semi-infinite domain $X > 0$. The remaining fraction of the energy in the initial state will evolve into a long-wave packet propagating along the right-running characteristic (i.e. directed toward increasing X). The slope of this characteristic curve varies in space and time as specified by the fixed standing wave, just as illustrated schematically in figure 1. The initial condition for the extended KdV equation is composed of the residual isopycnal displacement obtained from the difference between the initial thermocline slope and the standing wave. After a small number of simulations it was found that to match the laboratory results, the initial energy should be partitioned equally between the background condition and the evolving soliary wave packet.

To compare the interface displacements predicted by the model (represented by (5.1) and (5.2)) with those measured by the ultrasonic wavegauges, it is necessary to introduce a number of *virtual* wavegauge positions in the very long model domain by unfolding the tank along the domain. To create a time series equivalent to the laboratory record the displacements from each of these virtual wavegauges are then summed. Figure 6 shows the model and laboratory time series for a simulation in which the amplitude of the initial disturbance was partitioned equally between the background seiche and the initial condition for the extended KdV equation. The model

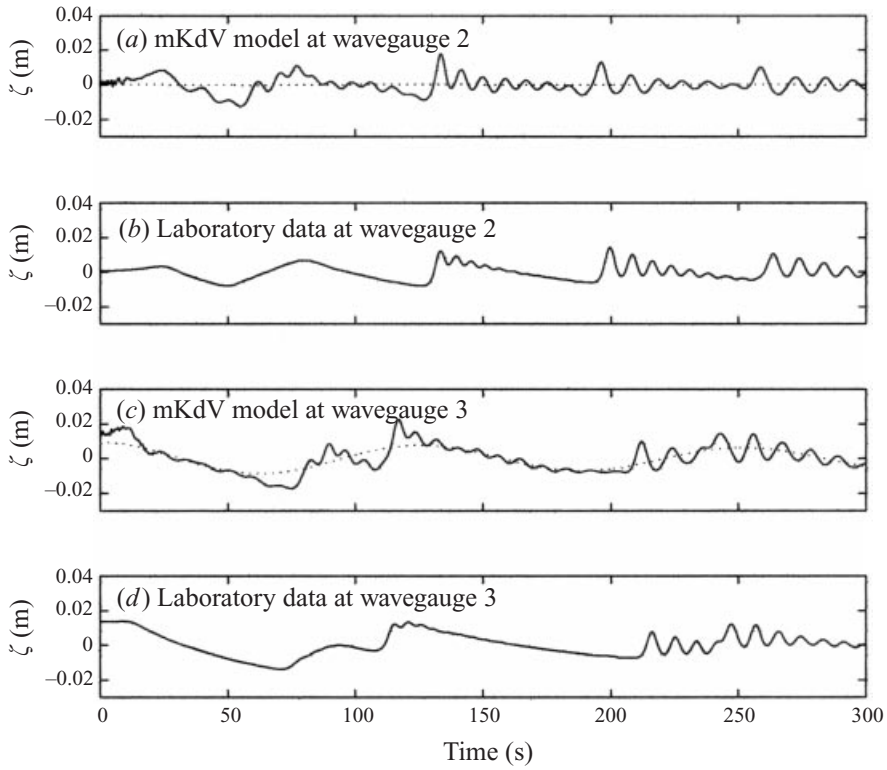

FIGURE 6. Time series of the interfacial displacements predicted by the KdV model and measured by the wavegauges at positions B and C are compared. The initial thermocline displacement was partitioned in such a way that 50% of the initial amplitude was assigned to the seiche mode and remaining displacement was assigned to the initial condition for the KdV model.

time series includes some high-frequency components introduced by the artificial step in the initial condition at $x = L$. However, these soon leave the domain after which the model interface displacements generally compare well with the laboratory observations. Although small variations in the arrival time of the packet front, the number of waves in the packet, and the amplitude distribution exist between the laboratory measurements and the simulation, further improvement of the numerical method, and especially the idealization of the initial conditions, would be expected to improve the simulation. From a practical standpoint, the key element is the splitting of the energy resident in the 'initial field' between the seiche field and the wave packet. We have not engaged in any systematic study of this effect to optimize the comparison between the model simulations and laboratory results. This partitioning of the energy between the two fields is likely to vary depending on the initial non-equilibrium slope of the interface and, perhaps, with the basin length. Nevertheless, there are some obvious influences of the seiche field on packet evolution that are captured quite well by the model.

5.2. *Evolution in a basin with variable depth*

We consider in this section the evolution of a long-wave packet in the presence of both space–time variations arising from a seiche and spatial inhomogeneity arising from a variable basin depth. In contrast with the previous section, the two terms proportional to $h_2'(x)$ appearing in the expression for the index of refraction $n(x, t)$ given by (4.5)

are now non-zero. As such, the low frequency of the seiche field alternately reinforces and relaxes the effect of variable depth, or vice versa depending on the initial phase relationship between the seiche and the initial condition for the evolving wave packet. Stated another way, the characteristic exhibited in figure 1 now oscillates about a curved mean position following the evolution of the packet, the mean curvature of the characteristic being determined by the variable basin depth.

The results presented here all correspond to a particular theoretical modification of the laboratory configuration shown in figure 5. The upper layer has a depth of 5.8 cm and the lower layer depth varies linearly from 23.2 cm at the left-hand end of the tank to 9.2 cm at the right-hand end. The initial condition, composed of a triangular distortion of the interface with peak amplitude 1.16 cm extending over 3 m (i.e. one-half of the tank length), was always released from the left end of the tank. The peak amplitude ratio for the initial condition is $\zeta_0/h_1 = 0.2$, and the lower-layer depths vary from $h_2/h_1 = 4$ at the left-hand end to $h_2/h_1 = 1.59$ at the shallow end on the right. We specifically avoid the situation where the leading-order part of the coeffiecient α of the nonlinear term (cf. (4.6)) passes through zero (i.e. a situation where the wave packet encounters the critical depth during its traverse of the basin). We expect that the presence of the background seiche field might play a very influential role in the transmission of a long wave packet through the critical depth, but we choose to relegate that to a separate study.

The seiche field imposed in the simulation presented here corresponds to the lowest mode defined by the physical optics approximation (cf. Bender & Orszag 1978) for a linear, standing wave in the variable-depth basin. The analytical form for this field, the results of which are needed to define the coefficient functions given in (4.3), (4.5), (4.6) and (4.7), is presented in Appendix C.† For convenience and illustrative purposes only, we choose the peak amplitude of the seiche field at the left-hand end of the basin to have the same value as the triangular initial condition at the same point. In this sense the energy partitioning between the seiche and wave packet fields is (approximately) equal. The phase of the seiche field relative to the initial condition for the packet, however, is allowed to vary.

Simulations of the KdV equation (3.10) emulating the evolution in a basin of linearly varying depth and length L were conducted by employing a computational domain consisting of a periodic continuation of the *double basin* obtained by means of a symmetric extension of the true basin about the position $x = L$. Hence, the simulated basin corresponds to one with periodically varying inhomogeneity, consisting both of a seiche field and a triangular topographic variation, with spatial period $2L$.

We first exhibit results corresponding to time series recorded by virtual wavegauges located in the positions shown in figure 5 when boundary layer dissipation effects are neglected. These time series are shown in figure 7 for three different initial conditions. Each column corresponds to time records from a specific gauge, varying from $x = L/4$ on the right, $x = L/2$ in the centre, and $x = 3L/4$ on the left. The centre row shows the evolution in the absence of any background seiche. The top row (*a*) reveals the evolution when the seiche is out of phase with the initial condition while the bottom row (*c*) shows corresponding records when the seiche is in phase with the initial condition. The influence of the seiche on long-wave packet evolution in the basin is quite profound. Both the amplitudes and the number of waves appearing in the resulting packet increase as one compares corresponding time series moving from the

† Appendix C is available from the Journal of Fluid Mechanics editorial office, Cambridge, and is posted on the website http://www.cwr.uwa.edu.au/~horn/papers/space-time.html.

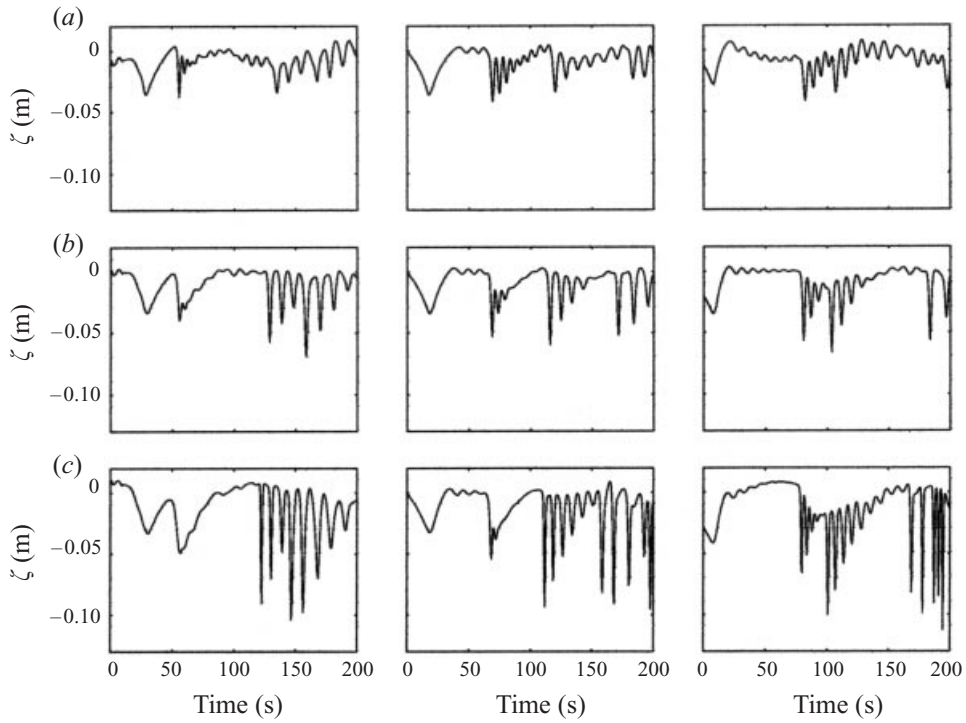

FIGURE 7. Each column contains time series predicted by the KdV model at wavegauge positions A, B, and C. Each row corresponds to the evolution resulting from the same initial condition, but with a different seiche condition. Row (*a*) Seiche out of phase with initial condition; (*b*) no seiche; (*c*) seiche in phase with initial condition.

top to the bottom rows. Results for identical initial conditions, but including boundary layer dissipation effects, are shown in figure 8. The energetics is clearly affected, but the qualitative differences arising from the seiche effect are still pronounced.

To illustrate the spatial structure of the packet evolving from the same set of initial conditions used for the simulations shown in figures 7 and 8, we present spatial records at evenly spaced time intervals in figure 9 for evolution in the absence of dissipation. Figure 9(*a*) displays the packet evolution when the seiche is out of phase with the initial condition while the seiche is in phase with the initial condition in figure 9(*c*). Figure 9(*b*) shows evolution at identical time intervals in the absence of any seiche. The effect of variable topography is clearly evident in figure 9(*c*), especially the lowest panel where the lead wave is decelerating and diminishing in amplitude while the separation between the second and third wave is enlarged because of their (approximate) position bridging the point of maximum depth. The different gradients of the sloping 'flat' portions between the leading three waves in the second-to-last panel of figure 9(*c*) is probably due to the local phase of the seiche. For purposes of comparison, the dissipative equivalent of figure 9(*c*) is shown in figure 10. Dissipation in this basin is clearly dominant after propagation over several basin lengths. The contrasting packet characteristics are strongly influenced by the presence and phase of the background seiche. It is apparent in this case of a thin upper layer considered here that, when the interfacial shear associated with the seiche is such that the lower-layer velocity is in the direction of the packet motion, the packet extracts energy from the background and grows. When the phase is reversed, the packet loses energy and

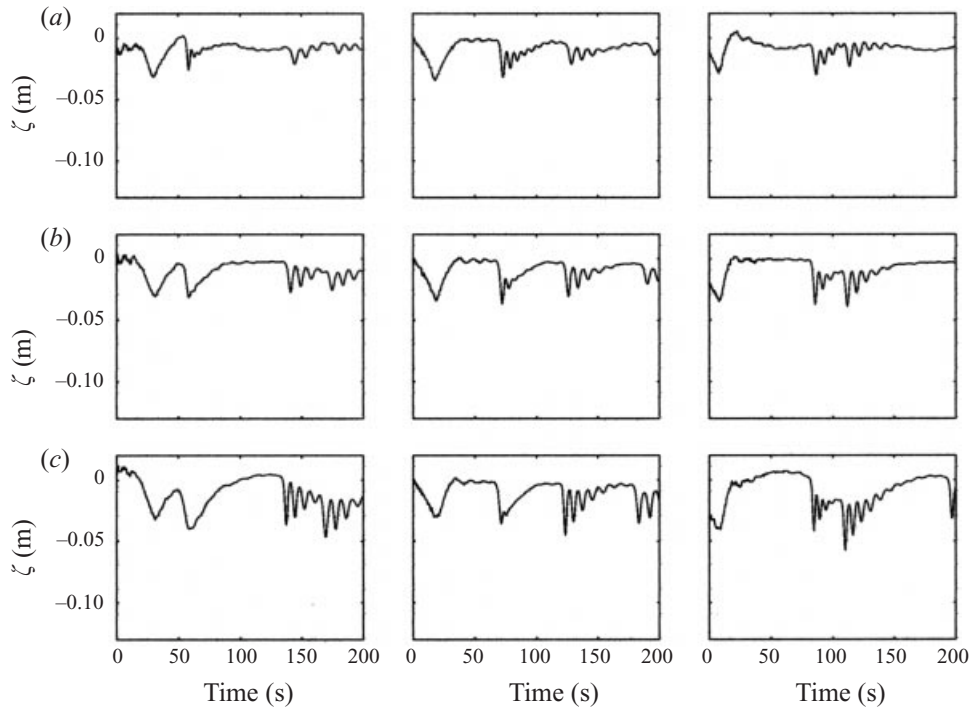

FIGURE 8. Same as figure 7 except that dissipative effects are included.

appears to contain a larger number of smaller waves (compare figures 9*a* and 9*b*). The present model is clearly deficient in regard to this coupling in that it precludes any energetics of the seiche field. Nevertheless, the influence of a space–time-varying background on the propagative characteristics of a long wave packet are captured and shown to be significant.

6. Summary

We have derived an extended KdV equation that describes the evolution of interfacial long waves in the presence of a strong, space–time varying background. In such a system the long-wave phase speed and the trajectory of the linear characteristic for local wave evolution vary slowly in space and time in accordance with the background state. The nonlinear and dispersive coefficients of the extended KdV equation are also variable and an additional term, $n(X, T)\zeta^{(1)}$, is introduced, where the index of refraction $n(X, T)$ contains space–time gradients of the background state. Approximate expressions are derived for the coefficients of the evolution equation for the case where the background state is composed of a moderate-amplitude ultra-long wave. Provision has been made for a spatially varying lower depth so that some topographic effects can also be included.

Implications of the extended KdV model were examined in the context of two specific applications in a basin of uniform depth: the evolution of an initial disturbance of the interface in the presence of a moderate-amplitude ultra-long wave in a very long basin, and the evolution of a tilted interface in a closed basin. It has been shown that the amplitude and the phase of the background ultra-long wave determines both the rate of steepening of an initial disturbance and the amplitude of the emerging

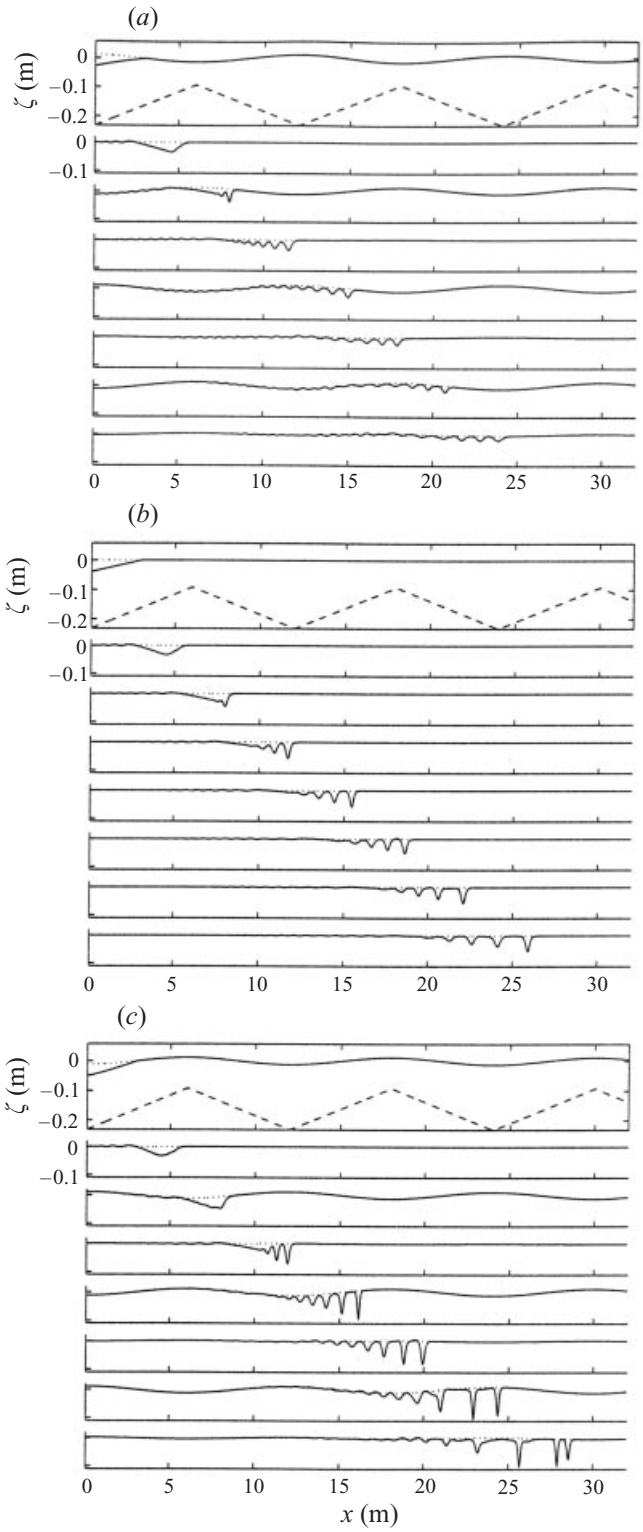

FIGURE 9. Spatial evolution of a long-wave packet at times $t = 0, 30, 60, 90, 120, 150, 180$, and 210 s for the same conditions described for figure 7. (*a*) Seiche out of phase with initial condition; (*b*) no seiche; (*c*) seiche in phase with initial condition.

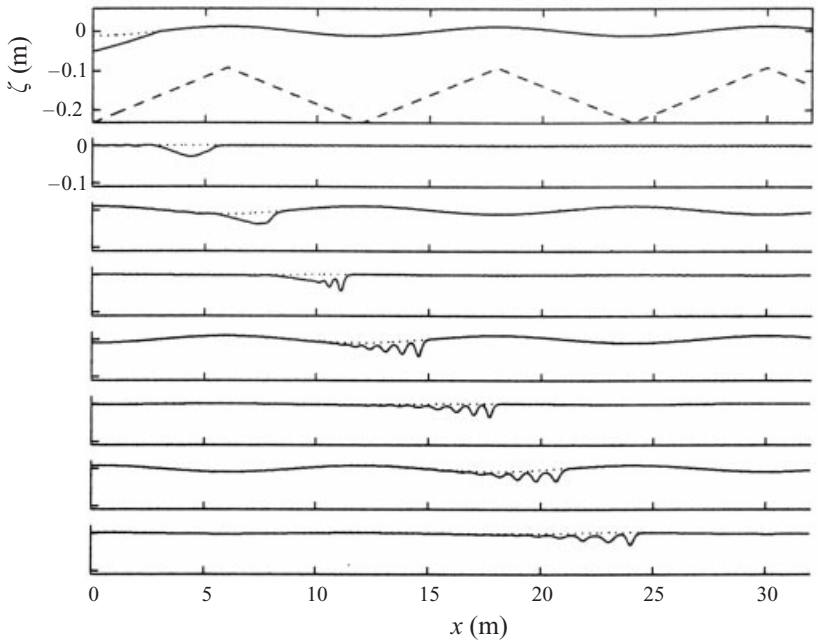

FIGURE 10. Dissipative evolution for the case shown in figure 9(*c*).

solitary waves. When an initial disturbance propagates on the crest of the background ultra-long wave (where the disturbance is a wave of elevation propagating on a thin lower layer) there is a transfer of energy from the background ultra-long wave to the evolving solitons. Conversely, when a local disturbance propagates in the trough of the background ultra-long wave it loses energy and reduces in amplitude. The extended KdV model was used to simulate a laboratory experiment in which an initial basin-scale standing wave steepens and evolves into a packet of solitary waves. The model shows that, if the energy of the initial basin-scale wave is partitioned so that half is retained as a background basin-scale wave and half is used as the initial condition, the model reproduces the main features of the evolving wave field.

The extended KdV model is expected to be a useful tool for the investigation of the evolution of weakly nonlinear waves in natural systems where the background state is rarely uniform or steady. For example, in lakes, solitary waves propagate in the presence of seiching motions; this was the motivation for the closed basin case considered above. Similarly, in fjords, solitary waves generated by tidal flow over a sill propagate into the fjord in the presence of strong tidal currents. When considering the shoaling and breaking of solitary waves, and the consequent dissipation and mixing, it is of significant importance to know the characteristics of the incident waves and of the wave packet. The extended KdV model reveals some important effects that a strongly varying background has on the characteristics of these waves.

However, this model only allows a one-way coupling in which, although the background field influences the evolution of a local disturbance, the local evolution does not modify the background field. A truly coupled system is necessary to capture the energetics of the full wave field, but the model developed here reveals the important role of the phase of the seiche field on local evolution and provides a simplified basis for exploring some of these subtle effects. In practical contexts where the amplitudes

of individual wave components stimulate benthic mixing, particle transport, etc., these apparent subtle effects may have very important consequences.

The second author acknowledges the assistance of the Gledden Trust in providing support via a Gledden Senior Visiting Fellowship at the University of Western Australia, and other partial support provided by the Office of Naval Research under Grant N00014-95-0041. This research was also supported by the Centre for Environmental Fluid Dynamics and the Austrilian Research Council. This paper is Centre for Water Research reference ED 1370 DH.

Appendix A. The extended KdV equation

Continuing the analysis to $O(\epsilon)$ in the asymptotic expansion of the dependent variables given in (3.1) leads to the following equation for the evolution of the leading-order displacement $\zeta^{(1)}(\theta, X, T)$ in the presence of a base state which is inhomogeneous in space and time:

$$
\begin{aligned}
&2\left[\rho_1\frac{C-U_1}{h_1-N}+\rho_2\frac{C-U_2}{h_2+N}\right]\left(\zeta_T^{(1)}+C\zeta_X^{(1)}\right)+\left\{\left[\rho_1\left(\frac{C-U_1}{h_1-N}\right)_T+\rho_2\left(\frac{C-U_2}{h_2+N}\right)_T\right]\right.\\
&\quad+\rho_1\left[2\frac{C-U_1}{h_1-N}C_X+C\left(\frac{C-U_1}{h_1-N}\right)_X\right]+\rho_2\left[2\frac{C-U_2}{h_2+N}C_X+C\left(\frac{C-U_2}{h_2+N}\right)_X\right]\Bigg\}\zeta^{(1)}\\
&\quad+\frac{3}{c}\left[\rho_2\left(\frac{C-U_2}{h_2+N}\right)^2-\rho_1\left(\frac{C-U_1}{h_1-N}\right)^2\right]\zeta^{(1)}\zeta_\theta^{(1)}\\
&\quad+\frac{1}{3c^3}\left[\rho_1(h_1-N)(C-U_1)^2+\rho_2(h_2+N)(C-U_2)^2\right]\zeta_{\theta\theta\theta}^{(1)}=0. \qquad \text{(A 1)}
\end{aligned}
$$

Observe that both $c(X,T)$ and $C(X,T)$ appear in the coefficients, and that the coefficient of the $\zeta^{(1)}$ term (enclosed by the brackets $\{\cdots\}$) contains space–time gradients of the background state represented by $C(X,T), U_{1,2}(X,T), N(X,T)$, and $h_2(X)$. The coefficients of the dispersive and nonlinear terms also vary on the evolution scales (X,T). When the background is spatially uniform and steady and the lower-layer depth is constant, the coefficient of $\zeta^{(1)}$ vanishes identically and the familiar constant-coefficient KdV equation is recovered.

REFERENCES

Ablowitz, M. J. & Segur, H. 1981 *Solitons and the Inverse Scattering Transform*. SIAM.

Apel, J. R., Holbrook, J. R., Lui, A. K. & Tsai, J. J. 1985 The sulu sea internal soliton experiment. *J. Phys. Oceanogr.* **15**, 1625–1651.

Bender, C. M. & Orszag, S. A. 1978 *Advanced Mathematical Methods for Scientists and Engineers*. McGraw Hill.

Djordjevic, V. D. & Redekopp, L. G. 1978 The fission and disintegration of internal solitary waves moving over two-dimensional topography. *J. Phys. Oceanogr.* **8**, 1016–1024.

Drazin, P. G. & Johnson, R. S. 1989 *Solitons: An Introduction*. Cambridge University Press.

Drazin, P. G. & Reid, R. H. 1981 *Hydrodynamic Stability*. Cambridge University Press.

Farmer, D. M. 1978 Observations of long nonlinear internal waves in a lake. *J. Phys. Oceanogr.* **8**, 63–73.

Farmer, D. M. & Smith, J. D. 1978 Nonlinear internal waves in a fjord. In *Hydrodynamics of Estuaries and Fjords* (ed. J. C. J. Nihoul), pp. 465–493. Elsevier.

Fornberg, B. & Whitham, G. B. 1978 A numerical and theoretical study of certain nonlinear wave phenomena. *Phil. Trans. R. Soc. Lond.* A **289**, 373–404.

GRIMSHAW, R. 1981 Evolution equations for long, nonlinear internal waves in stratified shear flows. *Stud. Appl. Maths* **65**, 159–188.

GRIMSHAW, R. 1998 Internal solitary waves in shallow seas and lakes. In *Physical Processes in Lakes and Oceans* (ed. J. Imberger), pp. 227–239. AGU.

HELFRICH, K. R. 1992 Internal solitary wave breaking and run-up on a uniform slope. *J. Fluid Mech.* **243**, 133–154.

HOLLOWAY, P. E. 1987 Internal hydraulic jumps and solitons at a shelf break region on the Australian north west shelf. *J. Geophys. Res.* **92**, 5405–5416.

HORN, D. A., IMBERGER, J. & IVEY, G. N. 2001 The degeneration of basin-scale internal waves in lakes. Submitted to *J. Fluid Mech.*

HUNKINS, K. & FLIEGEL, M. 1973 Internal undular surges in Seneca Lake: A natural occurrence of solitons. *J. Geophys. Res.* **78**, 539–548.

JOHNSON, R. S. 1973 On the development of a solitary wave moving over an uneven bottom. *Proc. Camb. Phil. Soc.* **73**, 183–203.

JOHNSON, R. S. 1997 *A Modern Introduction to the Mathematical Theory of Water Waves.* Cambridge University Press.

KAKUTANI, T. 1971 Effect of an uneven bottom on gravity waves. *J. Phys. Soc. Japan* **301**, 272–276.

KEULEGAN, G. H. 1948 Gradual damping of solitary waves. *J. Res. Natl Bur. Stand.* **40**, 487–498.

LEE, C.-Y. & BEARDSLEY, R. C. 1974 The generation of long nonlinear internal waves in a weakly stratified shear flow. *J. Geophys. Res.* **79**, 453–462.

MASLOWE, S. A. & REDEKOPP, L. G. 1980 Long nonlinear waves in stratified shear slows. *J. Fluid Mech.* **101**, 321–348.

MICHALLET, H. & IVEY, G. N. 1999 Experiments on mixing due to internal solitary waves breaking on uniform slopes. *J. Geophys. Res.* **104**, 13467–13478.

MILES, J. W. 1976 Korteweg–de Vries equation modified by viscosity. *Phys. Fluids* **19**, 1063.

MILES, J. W. 1981 The Korteweg–de Vries equation: a historical essay. *J. Fluid Mech.* **106**, 131–147.

MORTIMER, C. H. 1952 Water movements in lakes during summer stratification; evidence from the distribution of temperature in Windermere. *Phil. Trans. R. Soc. Lond.* B **236**, 355–404.

PELINOVSKIY, E., STEPANYANTS, Y. A. & TALIPOVA, T. G. 1995 Simulation of nonlinear internal wave propagation in horizontally inhomogeneous ocean. *Izv. Akad. Nauk. SSSR Fiz. Atmos. Okena* **30**, 77–83.

SPIGEL, R. H. & IMBERGER, J. 1980 The classification of mixed-layer dynamics in lakes of small to medium size. *J. Phys. Oceanogr.* **10**, 1104–1121.

THORPE, S. A., HALL, A. & CROFTS, I. 1972 The internal surge in Loch Ness. *Nature* **237**, 96–98.

THORPE, S. A., KEEN, J. M., JIANG, R. & LEMMIN, U. 1996 High-frequency internal waves in Lake Geneva. *Phil. Trans. R. Soc. Lond.* A **354**, 237–257.

ZHOU, X. & GRIMSHAW, R. 1989 The effect of variable currents on internal solitary waves. *Dyn. Atmos. Oceans* **14**, 17–39.